CC BY

EGU2016-8346

2D Pn Velocity-Gradient and Attenuation Models for Eurasia

Xiaoning Yang and W. Scott Phillips

Los Alamos National Laboratory, Los Alamos, New Mexico 87545, USA, xyang@lanl.gov

Los Alamos NATIONAL LABORATORY EST. 1943

Introduction

Pn is one of the most important phases in nuclear-explosion monitoring. Pn velocity-gradient and attenuation play important roles in shaping the Pn propagation both in terms of its travel time, which is used to locate events, and in terms of its amplitude, which is used for discrimination. Accurately mapping the lateral variation of Pn velocity gradient and attenuation will improve the monitoring of nuclear explosions through better predictions of Pn travel times and amplitudes.

In this study, we develop 2D Pn velocity-gradient and attenuation models for Eurasia using observed Pn travel times and amplitudes. We first calculate average P-wave velocity gradients for each Pn path from observed Pn travel times incorporating predictions from a 3D Earth model. We assume that these path-specific gradients are the mathematical mean of laterally varying velocity gradients along the paths. The assumption is validated through a Monte Carlo simulation. Using a tomographic inversion, we construct a 2D P-wave velocity-gradient map from path-specific velocity-gradient measurements.

To invert for the 2D Pn attenuation model, we correct observed Pn amplitudes for geometric spreading using predictions from the 2D Pn velocity-gradient model we just developed. The Pn velocity-gradient model from observed data allows us to make realistic Pn geometric-spreading corrections, which in turn results in more accurate Pn attenuation models.

Pn Velocity-Gradient Model

1 Problem Formulation

Pn travel path

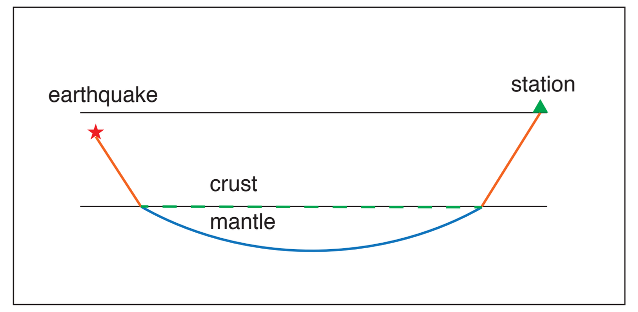

Pn travel time *TT* between an earthquake *i* in the crust and a seismic station *j* on the free surface can be represented as the summation of Pn travel times in the crust, the travel time of the head wave along the Moho and the contribution due to the P-wave velocity gradient in the uppermost mantle:

$$TT_{ij} = T_c + T_h + T_g \qquad (1)$$

Subscripts c, h and g in (1) represent crustal components, the head wave and the gradient respectively. For an uppermost mantle with a velocity gradient g that does not change much either vertically or horizontally, the last term in (1) can be approximated as:

$$T_g = A_{ij} g_{ij}^2 \qquad (2)$$

Here g_{ij} is the path-averaged velocity gradient between earthquake i and station j. A_{ij} is a linear function of $-L^3$ where L is the Pn path length between Moho piercing points. As L increases, A_{ij} decreases.

For each observed Pn travel time TT, we predict T_c and T_h in (1) from a 3D upper-mantle velocity model, subtract them from TT, and solve for path-specific g using (2). We assume that the path-specific g is the mean of laterally varying Pn velocity gradients along the path. For a discretized path, it is expressed as:

$$g_{ij} = \frac{1}{L} \sum_k \sum_p g_p c_{pk} \Delta_k \qquad (3)$$

where Δ_k is the length of the kth discretized path segment. g_p is the velocity gradient at model node p. c_{pk} is a weighting coefficient. With (3), a system of linear equations can be formed from multiple measurements. A 2D Pn velocity-gradient map can then be constructed through a linear tomographic inversion.

2 Assumption Validation

To validate the assumption of equation (3) that a path-specific P-wave velocity gradient is the mean of the laterally varying velocity gradients along the path, we performed a Monte Carlo simulation. We constructed a 2D Earth model with laterally varying velocity gradient. The model is composed of 10 equal-width regions with the same velocity of 8.1 km/s at the top, but with different vertical velocity gradients. In the simulation, the travel time between a source and a receiver at the two top corners of the model is calculated repeatedly. During each calculation, the order of the regions is shuffled randomly. The figure at the lower left shows two realizations of the model. The figure at the lower right plots the results from 10,000 calculations as a histogram. The red line in the figure marks the travel time calculated from a model with a single velocity gradient that is the mean of the gradients of the models on the lower left. The travel time is very close to the peak location of the travel-time distribution from the Monte Carlo simulation. The dashed green line is the travel time from a model constructed using a different assumption. (See the figure caption for details.) The result is much more biased.

Two example velocity models for MC simulation

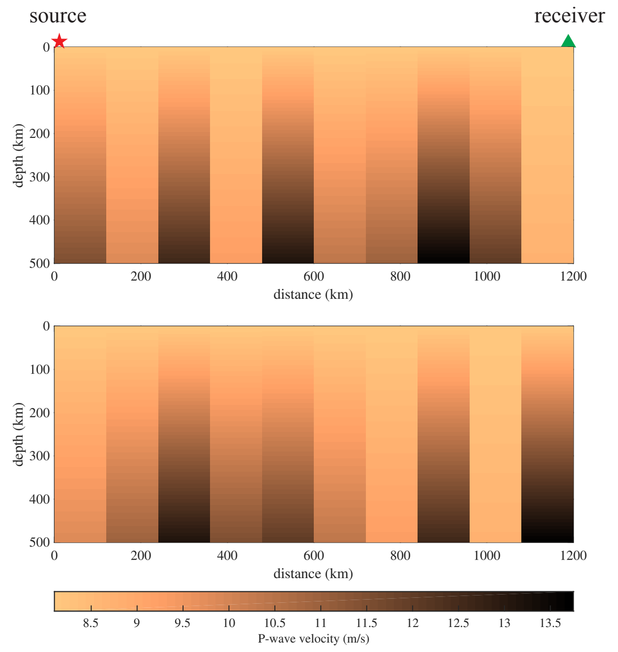

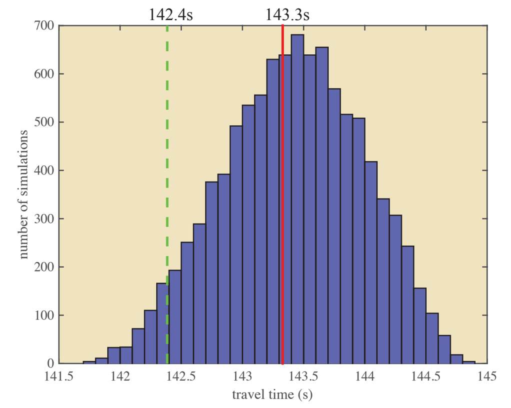

Distribution of travel times from the Monte Carlo simulation. The mean of the distribution is 143.4s. The red line marks the travel time for a model with a single velocity gradient calculated as the mean of the laterally varying gradients. The green line marks the travel time for a model where the gradient is calculated as the square root of the mean of squares of the laterally varying gradients.

3 Pn Travel-Time Measurements

Pn travel times from more than 5,000 earthquakes and explosions recorded by about 4,500 stations throughout Eurasia are collected. Epicentral distances of the dataset are between 2˚ and 15˚. The dataset contains measurements reported in bulletins as well as measurements made by U.S. national laboratory scientists. The total number of measurements is about 85,000. Because of the uneven distributions of earthquakes and stations, the path-density distribution (the figure in the lower left) is not uniform. In general, Pn path density is high in tectonically active regions due to large numbers of earthquakes and stations in those regions. This is particularly true for southern Europe, where the Pn path density is the highest.

Pn travel-time path density

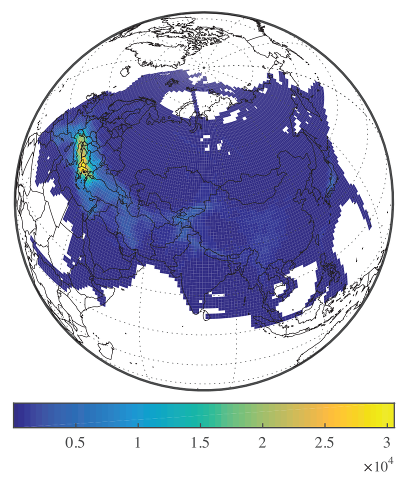

The figure on the right plots the calculated T_g term in equation (1) from measured Pn travel times. According to equation (2), T_g should always be negative and decreases with increasing distance. Smaller T_g correspond to higher velocity gradients in the uppermost mantle.

These T_g measurements are used to calculate path-specific P-wave velocity gradients with equation (2), which then make up the input data for the tomographic inversion of the 2D P-wave velocity-gradient model based on equation (3).

T_g

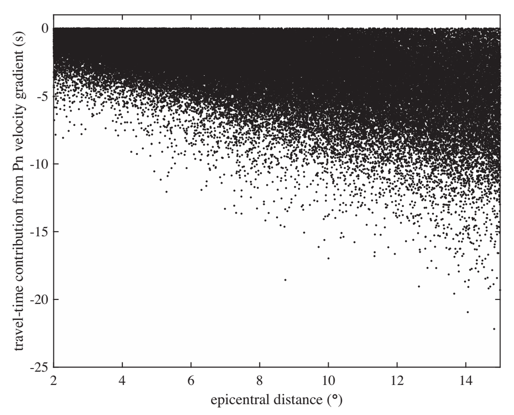

4 Pn Velocity-Gradient Model Inversion

For the tomographic inversion of the velocity-gradient model, we discretize the Earth using a triangular tessellation. We first define an active region where we have data coverage. We then construct the mesh using variable-resolution discretization. Within the active region, the node spacing is 1˚. Away from the active region, the spacing progressively increases. The figure below shows the mesh tessellation. During the inversion, only nodes that contribute to the calculation of path-specific velocity gradients are included.

Tessellation mesh for the inversion

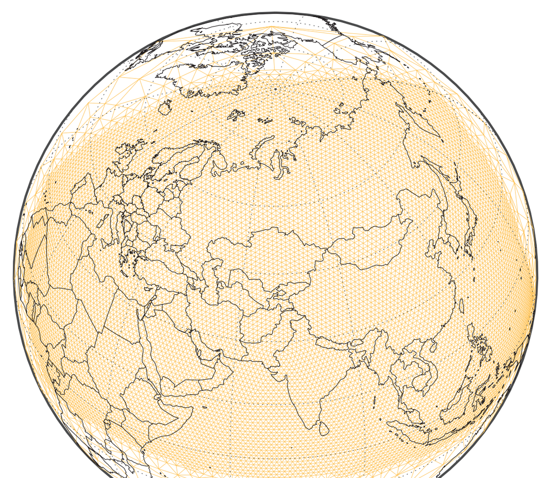

We employ a Bayesian approach in a damped and weighted least-squares inversion to invert for the gradient model. We use the right-hand-side of equation (3), to derive an *a* priori model for the inversion. We first sum c_{pk} for each node over all paths. We then replace g_p on the right-hand-side of the equation with g_{ij} on the left-hand-side for each measurement and sum $g_{ij}c_{pk}$ for each node over all paths. The *a priori* model is obtained by dividing the second summation by the first summation.

The figure to the right shows the velocity-gradient model from the inversion. Also plotted are tectonic plate boundaries. The velocity gradient is almost universally positive for the whole Eurasia. Much of the gradient variations occur along plate boundaries under overriding plates. It indicates that strong velocity-gradient variations and the presence of complex tectonic processes may be related. The highest gradient is observed in the Caucasus region between the Black Sea and the Caspian Sea. Other regions of higher gradient include the Scandinavia region, western and southern Iran, the Hindu Kush and western part of the Himalayas. Except the Scandinavia region, all other regions of high velocity gradient are tectonically active regions.

The figure below compares the data residual from the *a priori* model prediction (blue) and that from the inverted model prediction (red). The residual from inverted model prediction is more normally distributed.

Data misfit residuals

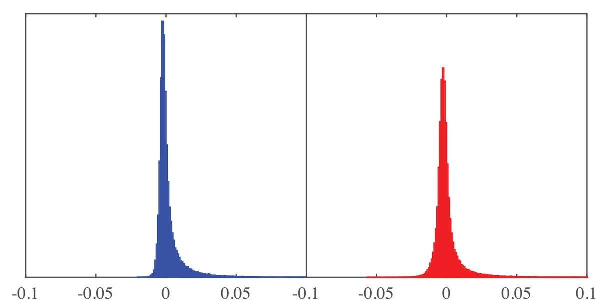

Pn velocity-gradient model from inversion

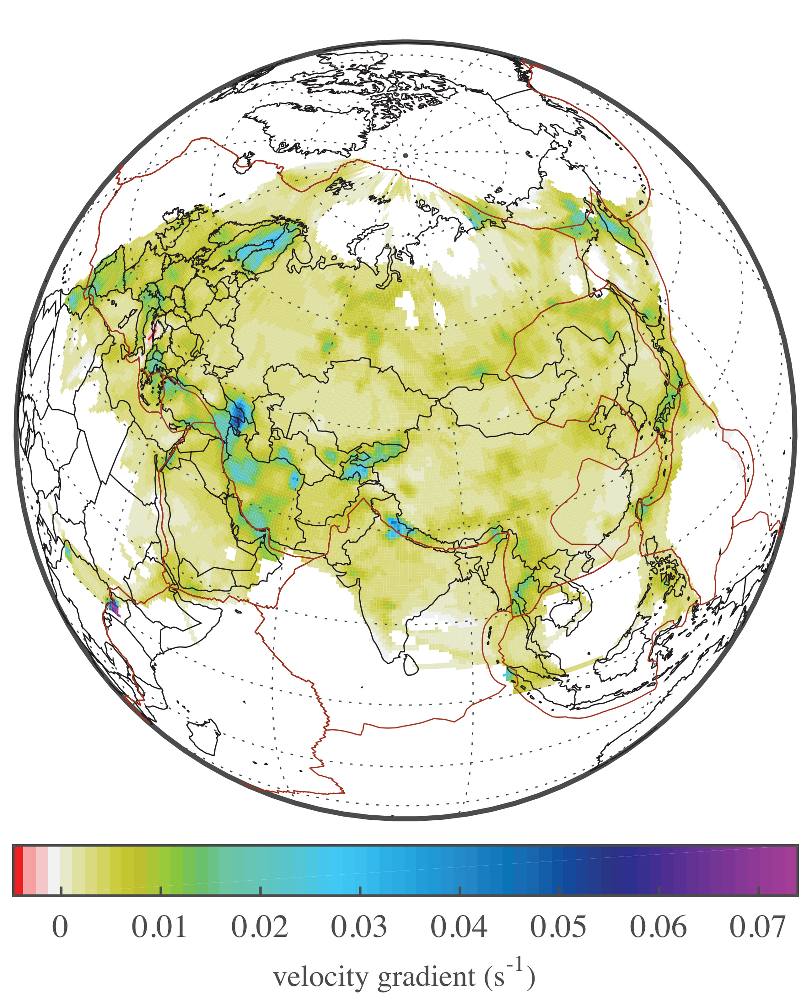

Pn Attenuation Model

Using the 2D Pn velocity-gradient model, we predict the Pn geometric spreading between stations and earthquakes. We use the prediction to correct Pn amplitude for spreading. The corrected amplitudes are then used in a tomographic inversion to develop Pn attenuation models at multiple frequencies. The figure below gives an example of geometric-spreading corrected amplitudes plotted as a function of distance. Figures to the right show the resulting Pn attenuation-coefficient models from the inversion at 4 frequencies. Overall the attenuation increases with frequency. Large attenuation variations tend to occur in tectonically active regions. This is more apparent at lower frequecies.

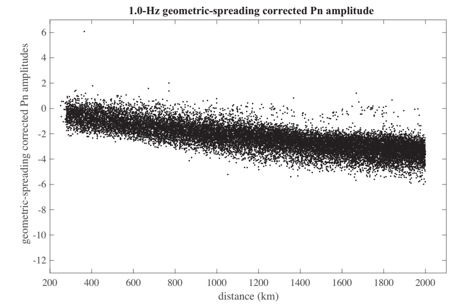

Because of the uneven spatial sampling of Pn paths, we adopted a similar model tessellation method as what we used in the velocity-gradient model inversion. The figure below shows the variable-grid tessellation based on Pn amplitude path density.

Tessellation mesh for the inversion

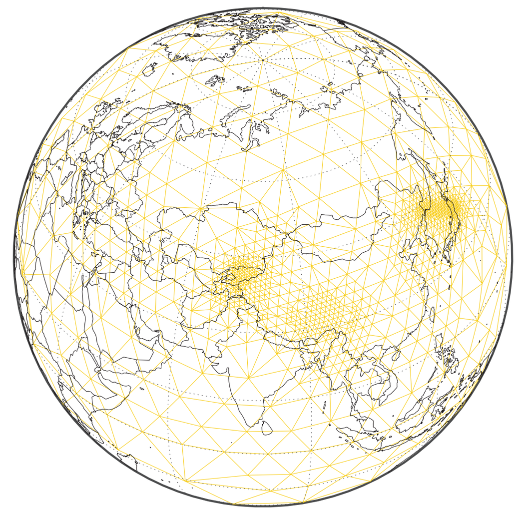

Multi-frequency Pn attenuation-coefficient model

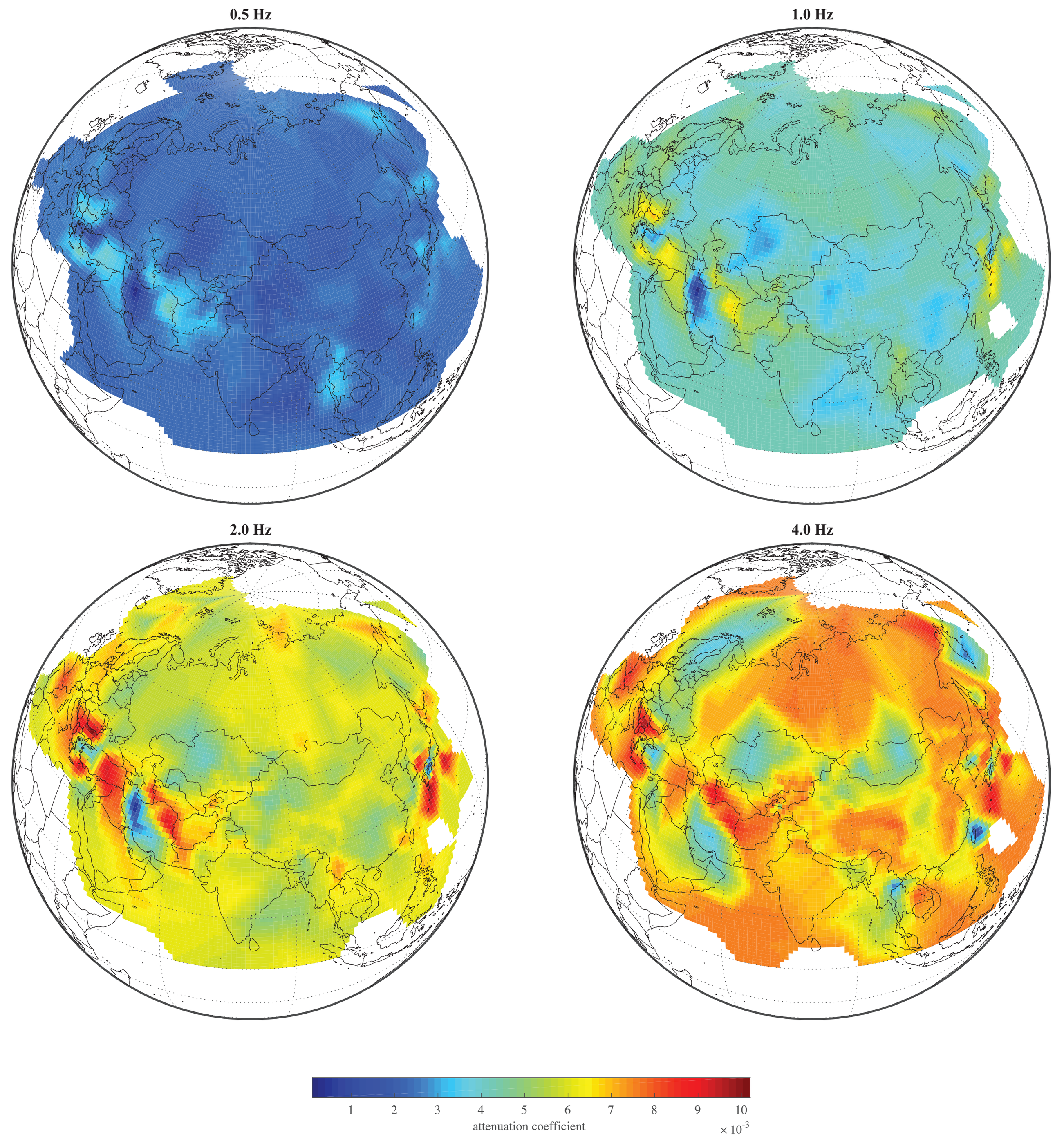

Conclusions

We develop 2D Pn velocity-gradient and attenuation models for Eurasia based on observed Pn travel times and amplitudes. The travel times are corrected for crustal and head-wave components to isolate the velocity-gradient contribution for path-specific velocity gradient calculation. The assumption that these path-specific velocity gradients are the mean of the laterally varying velocity gradients along the paths is validated through a Monte Carlo simulation. A tomographic Pn velocity-gradient model is then derived using a linear Bayesian inversion approach. The model is well resolved in tectonically active regions. The velocity gradient is positive almost everywhere. Large gradient variations are observed mainly along plate boundaries under overriding plates.

Using the 2D Pn velocity-gradient model, we predict the geometric spreading of Pn amplitudes. We remove the spreading effect from observed Pn amplitudes and invert the corrected amplitudes for 2D tomographic Pn attenuation models at multiple frequencies from 0.5 to 8 Hz. Large attenuation variations are seen in tectonically active regions, particularly at lower frequencies. For high frequencies, attenuation variation is more widespread.

LA-UR-16-22316